Optimized nonlocal active sound control in frequency domain

DOI:
10.1016/j.apacoust.2021.108506

Document Version
Accepted author manuscript

Optimized nonlocal active sound control in frequency domain

N. Hu[1], S. Utyuzhnikov[1,2]

[1] University of Manchester, Manchester, M13 9PL, UK,

s.utyuzhnikov@manchester.ac.uk,

[2] Moscow Institute of Physics & Technology, Russia

Abstract

In the active sound control problem considered in the paper, a quite arbitrary closed region is acoustically shielded from ambient noise generated outside via implementation of secondary sound sources which are situated at the perimeter of the domain to be protected. It is presumed that the information available for the operation of control is only limited by the acoustic field that can be measured on a closed surface around the shielded region. The problem becomes much more complicated if there are desired sound sources situated inside the shielded region. In this case the input field is determined by contributions from noise, desired sound and controls. It is supposed that only the total acoustic field is available that makes the statement of the problem quite general and realistic. As the output, it is required to attenuate noise while preserving the desired field unaffected. To tackle the problem, a recently developed algorithm based on the nonlocal control is applied. From the point of view of a practical realization, the number of microphones and loudspeakers should be minimized. We propose for the first time some ways to essentially optimize distribution patterns of controls and sensors for the nonlocal control with preservation

of desired sound. Numerical experiments are carried out for noise attenuation in a cube to study the trade-off between the level of noise reduction and number of sensors and controls. It is demonstrated that the nonlocal control can be efficiently realized with a reasonable number of sensors and controls. As shown, with only two controls per wavelength the achieved level of noise attenuation exceeds 10 dB. This result matches the optimal local control when any desired sound is absent.

Key words: active sound control; noise attenuation; Calderón potential; nonlocal control; optimization; quadrature.

---

1 Introduction

Due to the increasing awareness of noise hazard in modern society, the active sound control (ASC) has been drawing soaring attention in decades as a perspective approach to attenuate audible noise. Based on the Huygens principle [1], this approach effectively reduces the noise level in a predetermined region by generating anti-noise with secondary sources (also called controls) situated at the perimeter. In the simplest one-dimensional unbounded interpretation with a monochromatic noise considered by Leug [21], the anti-noise corresponds to the wave having the same amplitude but the opposite phase. This leads to the noise cancelation. In practice, the ASC performs appreciable noise attenuation in low- or mid-frequency ranges [14]. However, it becomes ineffective along with growth of frequency, as plenty of controls and transient responses are required in high-frequency cases [2]. In contrast to the ASC, the passive sound control, which is characterized by hindering or absorbing sound waves via some special mechanical methods, represents an efficient way to attenuate noise in high-frequency range but it provides poor noise attenuation

at low frequencies [6]. Both two approaches can be combined, when it is appropriate, in order to achieve desirable noise reduction in broadband acoustic spectrum.

The traditional ASC systems are based on two principal algorithms: the feed-back and feed-forward controls [6, 24]. In the feed-back system, noise intensity is minimized nearby error sensors, which are located inside the shielded domain, via their immediate effect on the controls. In turn, in the feed-forward system, the noise cancelation is achieved with the use of the reference sensors placed outside the shielded domain [10]. The filtered-x least mean squared (FxLMS) algorithm considering the secondary-path effects is the basic technique which is applied in both two systems. In addition, the adjustable-step-size LMS, Kalman, Newton, or recursive-least-squares (RLS) algorithms allow the convergence rate to be improved, which might be slow for FxLMS in some circumstances [14]. The conventional feed-forward ASC approaches are based on prediction of noise propagation and often require detailed information such as the characteristics associated with the noise source, medium of propagation, boundary conditions, Green function, etc. Such requirements severely constrain practical applications of ASC methods.

Apparently, Fedoryuk [5] and Malyuzhinets [22] were the first who formulated the ASC problem on a strict mathematical level. Apart from noise generated outside the protected region, he included the internal sound field which is interpreted as a desired sound. He presumed that the total sound field from the primary sources is available at the perimeter of the shielded domain. In [5] the solution to the problem is obtained on a quite arbitrary Gaussian surface for which the Huygens principle is supposed to be valid. Such a surface is sometimes called the Huygens surface. As shown in [18], the contribution to

the acoustic field of desired and undesired sources can be effectively split with the use of surface potentials of Calderón type thanks to the projection property. The problem of minimization of the acoustic strength for the controls is considered in [19] and [20] in both continuous and discrete formulations.

Under the same assumption of the primary field availability, the problem is considered in [28] on a discrete level with the use of the formalism developed in the Method of Difference Potentials (DPM), which is assigned to a discrete space selected. Afterwards, this approach is demonstrated to be applicable for unsteady problems in [32]. General solution to the ASC problem in both differential and finite-difference formulations is obtained in [33, 34]. In addition, the DPM-based approach is successfully extended to composite domains [30, 31, 40]. Quite general unsteady formulations are considered in [29, 39]. The developed theoretical algorithms are implemented in a series of physical experiments in [15–17].

The link between the finite-difference and continuous formulations is clearly shown in [36]. The approach based on surface potentials in the continuous formulation is successfully extended to unsteady formulations in [38] and nonlinear ASC problems in [40] where unsteady and nonlinear potentials are introduced, respectively. Numerous numerical experiments with discrete controls based on the approximation of surface potentials are carried out in [25, 26] for single and composite domains, respectively. It is to be noted that for a plane, sphere and ellipsoid the problem of minimization of the number of controls is addressed in [11, 12, 24]. The presence of desired sound is not considered there. It is concluded that with only two controls per wavelength essential noise attenuation can be achieved. This result is remarkable since such a sparse grid is not sufficient for the wave resolution.

The key drawback of the problem formulation, which is used in [5, 18, 28] and many other papers cited above, is the assumption of the total primary field to be available at the perimeter of the protected domain. It turns out that in this case, thanks to the Huygens principle, a local control can be applicable provided that a sufficient number of controls is present. However, the assumption of the primary field availability is usually not valid for the real-life control because of contribution of the secondary sources. This reverse effect is especially damaging in case a desired sound is present. The problem is that, as shown in [33], in the steady formulation the level of desired sound is doubled outside the shielded domain thanks to the effect of the secondary sources. Thus, the contribution of purely primary sources is often unavailable (see [41] in more detail). To overcome this problem, directional measurements and surface integral control can be used [4, 13, 27]. However, the field of applications for these techniques is quite limited [7–9]. It turns out that the problem can be effectively resolved with the use of nonlocal active sound control (NASC) first proposed by Utyuzhnikov in [37] for steady problems. This idea is extended to unsteady problems in [41]. In contrast to the local control, two separate Huygens surfaces are required for sensors and controls, respectively. As a result, the locations of sensors and controls do not coincide.

A practical algorithm for real-time implementation of NASC is proposed in [42]. Zhou and Utyuzhnikov have recently realized this algorithm in both frequency and time domains in [44, 45], respectively, and carried out numerical experiments including sensitivity analysis. In particular, it is shown that in the case of sparse distributions of the sensors and controls, the nonlocal control can provide much greater noise attenuation than the local control even if the primary field is supposed to be available. More precisely, this effect occurs

if the desired sound component is present and essential enough. As noted in [44], with a sparse distribution of sensors and controls the projection property of the potentials can be corrupted.

In papers [44, 45], the authors consider an uniform distribution of the sensors and controls to protect a cubic domain. Thereby, no attention is paid to the optimization of the number of sensors and controls apart from their total uniform reduction in the framework of the sensitivity analysis. As a result, too many controls and sensors per unit surface might be required for a practical realization. Thus, the result achieved is still far away from economically viable applications, for example, related to noise reduction in vehicle cabins, airplane cabins, elevators or meeting rooms.

The main objective of the current paper is to reduce the number of controls and sensors in the NASC problems while retaining the same noise attenuation level. Numerical experiments demonstrate a significant reduction of the number of control units in comparison to the ordinary uniform distribution. The paper is organized as follows. The general mathematical formulation of the ASC problem is given in Section 2. In Section 3 a formal solution to the ASC formulated in the previous section is provided. At the end of the section the algorithm of NASC with continuous distributions of sensors and controls, which are supposed to be acoustically transparent, is formulated. In the next section the algorithm is realized with a discrete distribution of sensors and controls. Possible ways to minimize the total number of control units are discussed there. In Section 5 the results of numerical experiments are shown which demonstrate the efficiency of the proposed distributions of the sensors and controls. Finally, the Conclusion is given in Section 6.

2 General statement of Active Sound Control problem

We define a spatial domain D: $\overline{D} \subseteq \mathbb{R}^3$. Within domain D, a bounded sub-domain D^+: $\overline{D^+} \subset D$ is regarded as the protected domain. Then, another sub-domain D^- can be described as: $D^- := D \backslash \overline{D^+}$. The boundaries of D and D^+ are noted by Γ_0 and Γ, respectively (see Fig. 1). They are supposed to be smooth enough to satisfy the Lipschitz condition.

Consider the formulation of the ASC problem in the frequency domain. First, we introduce the Helmholtz differential operator:

$$L := \Delta + k^2,$$

where k is the wave number.

Then, assume that the sound field in domain D is described by the following boundary value problem (BVP):

$$\begin{aligned} Lp &= g, \\ p &\in \Xi_D. \end{aligned} \tag{1}$$

Here, p is the Fourier image of the sound pressure, the source term g represents the primary acoustic sources corresponding to superposition: $g = g^+ + g^-$, in which g^+ and g^- are desired sound and noise sources, respectively: $\operatorname{supp} g^+ \subset D^+$, $\operatorname{supp} g^- \subset D^-$. Finally, Ξ_D is a function space such that the solution to BVP (1) is unique.

Since the problem is linear, the desired sound field can be determined by BVP:

$$Lp^+ = g^+, \tag{2}$$
$$p^+ \in \Xi_D.$$

In the ASC problem we need to find a control source G_0 such that the solution of BVP

$$Lp_c = g + G_0, \tag{3}$$
$$p_c \in \Xi_D,$$
$$\operatorname{supp} G_0 \in \Gamma$$

satisfies condition

$$p_{cD^+} = p^+_{D^+}. \tag{4}$$

Thus, the ASC is reduced to an inverse source problem. Condition (4) means that the desired sound field is retained while the noise must be canceled in the protected region D^+.

In the next section we provide formal solutions to the problem of ASC which can be achieved via local and nonlocal controls.

3 Solution of the inverse source problem

3.1 Local control with the use of surface potentials

If the primary field is supposed to be somehow available, the ASC can be realized with the use of local control under assumption that Γ is a Huygens

surface (see e.g. [18, 39, 42]). Indeed, presumes first that Green's function Gr to the problem is available.

Then, consider control given by

$$G_0 = \frac{\partial p}{\partial \boldsymbol{n}}_{|\Gamma} \delta(\Gamma) - p_{|\Gamma} \frac{\partial \delta(\Gamma)}{\partial \boldsymbol{n}}, \tag{5}$$

where $\delta(\Gamma)$ is the surface delta-function assigned to Γ, $\boldsymbol{n}$ is the outward normal to Γ. Thus, the control is fully determined by the sound pressure and its normal derivative at the boundary Γ.

From Green's formula, it follows that control (5) generates in domain D^+ field p_g that can be interpreted as "anti-noise" [43], which is a superposition of single-layer and double-layer potentials:

$$p_g(\boldsymbol{x}) = -\int_\Gamma (p_{|\Gamma} \frac{\partial Gr}{\partial \boldsymbol{n}} - Gr \frac{\partial p}{\partial \boldsymbol{n}}_{|\Gamma}) d\sigma = -p^-(\boldsymbol{x}), \quad \boldsymbol{x} \in D^+. \tag{6}$$

Here $\boldsymbol{x}$ corresponds to the observation points.

A more general control can be realized with the use of Calderón-Ryaben'kii's potential [37]:

$$P_{D^+} \boldsymbol{\xi}_\Gamma(\boldsymbol{x}) = \int_\Gamma (\frac{\partial Gr}{\partial \boldsymbol{n}}(\boldsymbol{x} \mid \boldsymbol{y}) \xi_{\Gamma|1}(\boldsymbol{y}) - Gr(\boldsymbol{x} \mid \boldsymbol{y}) \xi_{\Gamma|2}(\boldsymbol{y})) d\sigma, \tag{7}$$

where $\boldsymbol{x} \in D^+$, $\boldsymbol{\xi}_\Gamma = (\xi_{\Gamma|1}, \xi_{\Gamma|2})^T$.

It is clear that potential (7) coincides with (6) up to the sign if

$$\boldsymbol{\xi}_\Gamma = \mathrm{Tr}_\Gamma \, p_{D^+}, \tag{8}$$

where Tr is the trace operator:

$$\mathrm{Tr}_\Gamma \, w_{D^+} = (w_{|\Gamma}, \frac{\partial w}{\partial \boldsymbol{n}}_{|\Gamma})^T, \tag{9}$$

and w is any smooth enough function determined on D^+.

It is to be noted that generalized potential (7) can be calculated with the use of DPM [**?**] without the knowledge of Green's function. From the projection property of this potential it immediately follows that

$$P_{D^+} \operatorname{Tr} p_{D^+} = p^-_{D^+}. \tag{10}$$

Thus, surface potential (7) plays the role of a filter. It helps automatically remove component p^+ from the input data, reserving p^- as the target to attenuate. The same projection can be obtained with the use of Green's formula based on Green's function.

As can be seen, control (5) is entirely local. Therefore, it can be realized relatively easily. The key drawback of this approach is that it requires the primary field to be available at the control boundary Γ. In real-life applications, this field is not usually available since the acoustic field to be measured is strongly affected by the control itself. It can be shown that control (5) doubles the desired field immediately outside Γ in D^- (see [37]). Thus, due to the action of the control, the acoustic field becomes discontinuous across the boundary Γ and the primary field becomes unreachable. What even more important factor is that as demonstrated in [44], control (5) has the key property of projection only if it is continuously distributed on the Huygens surface. Otherwise, an extra uncontrollable contribution from the desired sources appears at the boundary field to be measured due to the error in the projection, and it can severely deteriorate the local control. It is worth noting that this kind of error cannot be determined in the entirely discrete formulation used in [28].

3.2 Nonlocal control

The problem related to the fail of the local control in the presence of a desired sound component can be effectively resolved with the use of the nonlocal control [42, 44, 45].

In the nonlocal control, sensors are supposed to be set on a Huygens surface Γ^- outside region D^+. Let the domain bounded by Γ^- be D^+_- (see Fig. 2): $D^+ \subset D^+_-$ and $\Gamma^- \in D^-$.

From the projection property

$$P_{D^+_-} \operatorname{Tr}_{|\Gamma^-} p_{cD^+_-} = p^-_{D^+_-}. \tag{11}$$

Thus, the input data required for the local control

$$G_0{}' = \frac{\partial p^-}{\partial \boldsymbol{n}}_{|\Gamma} \delta(\Gamma) - p^-{}_{|\Gamma} \frac{\partial \delta(\Gamma)}{\partial \boldsymbol{n}}, \tag{12}$$

can be calculated from potential (11).

Then, control (12) generates annihilating field

$$p_{g'}(\boldsymbol{x}) = -\int_\Gamma (p^-{}_{|\Gamma} \frac{\partial Gr}{\partial \boldsymbol{n}} - Gr \frac{\partial p^-}{\partial \boldsymbol{n}}_{|\Gamma}) d\sigma = -p^-(\boldsymbol{x}), \quad \boldsymbol{x} \in D^+. \tag{13}$$

It is important to note that control (11), (12) depends on the entire acoustic field at surface Γ^-. In addition, the input field is not limited by the primary field. As demonstrated in [44] and [45], this kind of control is stable even in case a desired component is present.

As noted in [42], if Green's function is available, control (11), (12) can be formulated explicitly. Otherwise, it can be based on surface potentials which

can be either calculated or measured in advance.

4 Discrete distribution of sensors and controls. Its optimization

In practical applications of ASC, beyond one-dimensional, discrete distributions of sensors and controls are usually implemented. To optimize their distributions, we can consider the presentation of the potentials via surface integrals. Then, the problem of optimality is reduced to the problem of optimal distribution of nodes for computing surface integrals.

First, consider the case of local control, following [25]. For the distribution of controls, we divide surface Γ into non-interesting elementary segments $\Delta\sigma_i \ \ (i = 1, ..., N_c)$. Each control is allocated onto one of the segments. Then, the right-hand sides in equations (5) and (6) are approximated by:

$$p_g \approx -\sum_{i=1}^{N_c}[p(\boldsymbol{y}_i)\frac{\partial Gr}{\partial \boldsymbol{n}}(\boldsymbol{x_i}, \boldsymbol{y_i}) - Gr(\boldsymbol{x_i}, \boldsymbol{y_i})\frac{\partial p}{\partial \boldsymbol{n}}(\boldsymbol{y}_i)]\Delta\sigma_i, \tag{14}$$

$$G_0 \approx \sum_{i=1}^{N_c}[\frac{\partial p}{\partial \boldsymbol{n}}(\boldsymbol{x}_i)\delta(\boldsymbol{x} - \boldsymbol{x_i}) - p(\boldsymbol{x}_i)\frac{\partial \delta}{\partial \boldsymbol{n}}(\boldsymbol{x} - \boldsymbol{x_i})]. \tag{15}$$

As a result, single-layer controls are approximated by sets on monopoles, and double-layer controls are represented by sets of dipoles.

Next, for the nonlocal control, in addition, surface Γ^- is split into non-interesting elementary segments $\Delta\sigma_j \ \ (j = 1, ..., N_s)$. Sensors are situated on the corresponding segments.

Then, we can obtain input data for the control from

$$p^-(\boldsymbol{x_j}) \approx \sum_{j=1}^{N_s}[p_c(\boldsymbol{y}_j)\frac{\partial Gr}{\partial \boldsymbol{n^-}}(\boldsymbol{x_j}, \boldsymbol{y_j}) - Gr(\boldsymbol{x_j}, \boldsymbol{y_j})\frac{\partial p_c}{\partial \boldsymbol{n^-}}(\boldsymbol{y}_j)]\Delta\sigma_j, \tag{16}$$

where $\boldsymbol{x_j} \in \Gamma$, $\boldsymbol{y_j} \in \Gamma^-$, $\boldsymbol{n^-}$ is the outward normal to Γ^-.

In turn, the generated annihilating field is given by

$$p_{g'} \approx -\sum_{i=1}^{N_c}[p^-(\boldsymbol{y}_i)\frac{\partial Gr}{\partial \boldsymbol{n}}(\boldsymbol{x_i}, \boldsymbol{y_i}) - Gr(\boldsymbol{x_i}, \boldsymbol{y_i})\frac{\partial p^-}{\partial \boldsymbol{n}}(\boldsymbol{y}_i)]\Delta\sigma_i, \tag{17}$$

$$G_0{}' \approx \sum_{i=1}^{N_c}[\frac{\partial p^-}{\partial \boldsymbol{n}}(\boldsymbol{x}_i)\delta(\boldsymbol{x} - \boldsymbol{x_i}) - p^-(\boldsymbol{x}_i)\frac{\partial \delta}{\partial \boldsymbol{n}}(\boldsymbol{x} - \boldsymbol{x_i})]. \tag{18}$$

Then, the optimization problem is reduced to achieving the minimal number of sensors and controls subject to the same accuracy.

Our further analysis is restricted by the assumption of a cubic domain D^+. In turn, domain D^+_- is also supposed to be cubic.

First, to approximate the surface integrals, we consider an ordinary uniform (OU) distribution which was used in [44]. In this case, each side of the cube is covered by a uniform grid. Then, the control units are supposed at the grid nodes as shown in Fig. 3a. Apart from the OU grid, we consider a shifted uniform grid (SU) in which the nodes are shifted to the geometric center of each segment as can be seen in Fig. 3b.

Next, to optimize the distribution of nodes, we consider the Gauss-Legendre (GL), Chebyshev-Gauss (CG) and Tanh-Sinh (TS) quadratures. A brief information on these quadratures is provided in the Appendix, where two different forms of CG quadratures, CG1 and CG2, are also introduced. A distribution of nodes for each quadrature is shown in Fig. 4.

In the next section, we carry out numerical experiments to demonstrate the efficiency of different distributions of sensors and controls.

5 Numerical experiments and discussion

5.1 Experimental setup

In this section results of numerical experiments with ASC are discussed. First, similar to [44], consider a cubic domain D^+ with 1 m in length as the protected region, which geometric center coincides with the origin of a 3D Cartesian coordinate system. It is natural to presume that for the nonlocal control the control domain D_-^+ is also cubic with sides equidistant from the appropriate sides of cube D^+ such that the Hausdorff distance H_d between surfaces Γ and Γ^- equals 0.5 m. Afterwards, virtual primary sources, controls and sensors are implied in the ASC system. Suppose that the primary source is represented by a monopole and the entire domain D is unbounded. The noise source is situated at point (1.5 $m, 1$ $m, 1$ m) outside the protected region, and the desired sound source of the same strength is located at the center of the protected region.

It is to be noted that without desired sound, in the case of a point noise source and homogeneous boundary conditions, the level of relative noise attenuation does not depend on the strength of noise because the problem is scalable. The same property retains if the source of desired sound is identical to the noise source.

Consider first interval from 0 Hz to 200 Hz to be the frequency range for simulation. It is worth noting that the results presented for very low frequencies are rather formal and hardly achievable in a practical implementation.

The average noise attenuation level A_s is determined by formula:

$$A_s = \frac{1}{N_{obs}} \sum_{j=1}^{N_{obs}} 20\log_{10}|\frac{p^-}{p_c - p^+}|, \tag{19}$$

where (19), N_{obs} represents the number of observation points in the protected region.

With both sparse and fine grids on Γ, simulations with different distribution patterns are considered. The numerical results with both local and nonlocal controls highlight the effectiveness of the optimized algorithms. In addition, the minimal number of controls and sensors per wavelength to achieve essential noise attenuation is evaluated.

5.2 Sparse grid

Further, we measure the number of controls on each side of cubic domain D^+ by parameter n_c which represents the number of units in the projection onto each edge. Thereby, the total number of controls on each side equals n_c^2. In a similar way, we introduce parameter n_s to measure the number of sensors.

In the case of a sparse grid, we presume that n_c varies between one and five.

5.2.1 Local control without desired sound

The local control performs effectively in case desired sound is absent. First, consider the case of n_c equaled to three (see Fig. 5). In this figure and further, the value inside the parentheses for the TS distribution represents coefficient α used.

Regarding to the distribution patterns presented in Fig. 5, it is important to

note that the noise attenuation decreases monotonically and smoothly with growth of frequency. Besides, the curves are roughly equidistant to each other over the frequency range. Optimized distributions intensely enhance the level of noise attenuation in comparison with the OU approach. For example, at 100 Hz, more than 18 dB in noise attenuation is achieved with SU distribution, which is about 8 dB higher than that with the OU scheme. Within optimized distributions, the sequence of noise attenuation level from high to low is as follows: SU, GL, CG1, CG2 and TS patterns. Thus, the SU distribution enables us to reach the most significant noise attenuation in this case.

With the increase of n_c to five, a similar trend occurs with a surge in the level of noise attenuation. As can be seen in Fig. 6, the gaps between the optimized distributions and the OU distribution scheme become wider. In comparison to the OU approach, the SU distribution increases the level of noise attenuation by about 13 dB with the same number of controls. Furthermore, the descending order of distributions based on the level of noise attenuation retains the same. The SU pattern provides about $4-6$ dB higher noise attenuation than the other optimized schemes. Moreover, the CG2 distribution performs better than the CG1 distribution with about 1 dB increment in case n_c equals five.

In Fig. 7, noise attenuation is kept practically at the same level by implementing various number of controls for different distributions. As can be seen, the TS pattern, with $n_c = 5$ and 150 controls in total, is capable of achieving the same level of noise attenuation as the OU distribution with $n_c = 11$ and 726 controls in total. As a result, the number of controls can be reduced by about 80 %.

It is to be noted here that, as shown in [44], the local control becomes unachie-

vable with the presence of desired sound, especially with a sparse distribution of controls.

5.2.2 Nonlocal control

To demonstrate the efficiency of the nonlocal control, consider first the case of three controls along each axis with and without the interior desired sound source. In this case, the number of sensors along each axis n_s equaled to seven is appropriate for most distributions except for SU pattern where $n_s = 10$ is needed. Thus, the SU distribution requires a significantly greater density of sensors to represent the projection property of operator (11).

The number of sensors should exceed the number of controls in NASC for a twofold reason. First, the area of sensors is larger. Second, a good approximation of the integral over sensors is important since the integral plays the role of a projection. If the number of sensors is very low, the projection property is not realized and the operation of the control becomes inconsistent with the projection property and, hence, unpredictable.

As can be seen in Fig. 8, for each specific distribution, the noise attenuation level is practically the same regardless of the existence of desired sound. More precisely, the variation between the two cases with and without desired sound is less than 1 dB. Thus, in contrast to the local control, the efficiency of the nonlocal control is insensitive to the presence of internal desired source.

As can be expected, with the nonlocal control the optimized distributions demonstrate the same level of efficiency in noise cancelation regardless the presence of desired sound. For example, in the middle of frequency range,

with the SU distribution more than 18 dB in noise reduction is achieved in comparison to only 10 dB with the OU distribution with and without desired sound. The GL, CG1, CG2 and TS distributions also reach a significant improvement in noise attenuation in both cases, with and without desired sound. For the same frequency, the GL pattern reaches 15 dB in noise reduction with desired sound that is slightly higher than 14 dB and 13.5 dB for the CG and TS distributions, respectively. A similar tendency occurs without desired sound.

Next, extend n_c to five while keeping $n_s = 7$ for the GL, CG, TS and OU distributions. At the same time, the SU pattern is considered with n_s up to 20. As can be seen in Fig. 9, satisfactory noise attenuation is achieved in this case. The results without desired sound almost coincide with the results with desired sound. In comparison to $n_c = 3$, the level of noise attenuation grows up to 10.5 dB with the OU distribution at 100 Hz even if the desired sound is present. The noise attenuation with the SU distribution reaches 27 dB despite of the presence of the interior desired source with the increase of about 50 %. Meanwhile, the other optimized distributions demonstrate an extra increment from 3 dB to 6 dB. It is worth mentioning that the GL distribution reaches more than 22 dB in the noise attenuation at low frequencies that is the second best result among all distribution patterns. It can also be noted that the curves of CG1 and CG2 schemes tend to coincide at higher frequencies.

Next, let us keep the same level of noise attenuation with various numbers of sensors and controls for different distributions. If desired sound is present, as shown in Fig. 10a, NASC is able to provide the same level of noise attenuation in the case of GL distribution, with $n_c = 3$ and $n_s = 7$, and in the case of OU distribution, with $n_c = 9$ and $n_s = 11$. In other words, the noise attenuation

effect of the GL distribution with 54 controls and 294 sensors is identical to that obtained with the OU distribution with 486 controls and 726 sensors. In turn, without desired sound, under the same number of controls and sensors as the GL distribution mentioned above, the noise attenuation with the CG1 distribution nearly approaches the level obtained with the OU distribution for $n_c = 9$ and $n_s = 11$ (see Fig. 10b). Thus, as a result of optimization, the number of sensors and controls can be reduced by about 90% and 60%, respectively.

As noted above, when the grid on Γ is coarse, the SU scheme provides the best level of noise reduction among mentioned distributions. Fig.11 demonstrates dependence of noise attenuation obtained with SU distribution on the number of controls and sensors. The number of controls varies between two and five. For the nonlocal control, n_s exceeds n_c with a factor up to four. As can be seen, the level of noise attenuation significantly increases as the number of controls rises. In particular, for both local and nonlocal control, about 4 dB and 6 dB growth of the level of noise attenuation is achieved via the increase of n_c from two to three and from four to five, respectively. Thus, NASC completely removes the effect of desired sound on the noise attenuation even on a course grid.

However, it is also clear that for the sake of reserving the monotonicity of noise attenuation, the SU distribution requires much more sensors for nonlocal control in comparison to the other distributions. This flaw severely restricts a potential application of the SU pattern.

Whereas the GL distribution appears to be very efficient when n_s exceeds five. Thus, with the use of combined distribution SU-GL for the nonlocal

control, the disadvantage of excessive introduction of sensors needed for the SU pattern can be successfully overcome. In the proposed distribution, controls are placed on Γ according to the SU scheme, while sensors are located on Γ^- following to the GL procedure. In this way, not only high level of noise reduction is produced by controls but also the projection at Γ^- is achieved with a reasonable number of sensors. As a result, when n_c is equal to three and five, the combined distribution provides better noise attenuation than that with the purely GL distribution. Besides, this approach saves a considerable number of sensors in comparison to the plain SU distribution as can be seen in Fig. 12.

5.3 Fine grid

It can be concluded that $n_c = 6$ is a watershed for the controls on Γ. If $n_c < 6$, then the SU pattern provides the most effective noise attenuation with a sparse grid. However, if $n_c \geq 6$, then the GL scheme overcomes the SU distribution. This result is consistent with the general theory of discrete quadratures and can only be expected for a fine enough grid. In this section, we compare the attenuation effect for the SU and GL distributions with n_c equal to five and six in application to both the local and nonlocal control. In addition, noise attenuation for the SU and GL distributions is also studied in case $n_c = 7$ to demonstrate dependence of the gap between noise attenuation for these two patterns on n_c.

5.3.1 Local control without desired sound

First, consider the results with local control without desired sound shown in Fig. 13a. They are obtained for the GL and SU distributions with $n_c = 6$. Comparing Figs. 6a and 6b, we can see that the upsurge of noise attenuation is obtained with the GL distribution when n_c reaches the value of six. At the same time, the level of noise attenuation with the SU distribution just slightly increases with the increase of the number of controls. For example, at 100 Hz, the noise reduction with the GL distribution reaches nearly 30 dB when $n_c = 6$ that is 8 dB higher than that value for $n_c = 5$. In contrast, only 1 dB increment is achieved for the same conditions with the SU distribution.

With $n_c = 7$, the level of noise attenuation based on the GL distribution continues to rise very significantly, achieving 35 dB at 100 Hz. Meanwhile, a finer SU grid does not give any essential improvement. Thus, the gap between the GL and SU distributions is further enlarged exceeding 7 dB.

5.3.2 Nonlocal control

Similar to the tendency noted for the local control, with NASC the GL distribution also demonstrates better results than the SU scheme in the case of a fine grid. As shown in Figs. 13c and 13d, if desired sound is present, similar levels of noise attenuation are achieved with the GL and SU distributions when n_c equals to six and seven. In addition, it is worth noting that the GL distribution not only provides more effective noise reduction than the SU approach but also allows much less usage of sensors. The same features occur with the nonlocal control if desired sound is absent as can be seen in Figs. 13e and 13f.

5.4 Minimal number of controls and sensors per wavelength

In this section, we estimate the minimal acceptable number of sensors and controls per wavelength. For this purpose, we extend the cubic side of protected domain to 1.75 m and the side of D_{-}^{+} to 5.25 m. The geometric centers of cubes D^{+} and D_{-}^{+} coincide at the origin. Then, we still retain the desired sound source at the origin but move the noise source to point $(10\ m, 0\ m, 0\ m)$. Afterwards, 5 controls and 15 sensors along each axis are allocated on Γ and Γ^{-}, respectively. Thereby, with the nonlocal control, the number of controls and sensors per wavelength appear to be equal.

As shown in Table 1, with the local control without desired sound, all distributions ensure good noise cancelation even with two controls per wavelength that is consistent with the results obtained in [11, 12] for smooth boundary surfaces. The SU distribution provides the best level of noise attenuation for different frequencies. Moreover, the CG2 distribution also performs well reaching 17 dB with four controls per wavelength.

In Tables 2 and 3, it can be seen that when the number of controls or sensors per wavelength equals to three, more than 10 dB attenuation can be provided with the optimized distributions.

With NASC, even when the number of controls or sensors per wavelength equals two, essential noise attenuation can be realized. For example, the SU and CG2 distributions still achieve 11.84 dB and 6.66 dB in noise reduction when desired sound is present.

6 Conclusion

The problem of optimization of the number of controls and sensors has numerically been studied in the frequency domain. Different distribution patterns have been analyzed for both local and nonlocal control to minimize the number of control units. Thanks to optimization, the number of controls and sensors can be drastically reduced in comparison to the ordinary uniform distribution. This effect is especially significant with the nonlocal control that makes the entire algorithm much more practicable.

It has been found that with a sparse gird of control units, a shifted uniform distribution provides the most effective noise attenuation. This means the optimal distribution pattern depends on the level of noise attenuation expected. For the level of about 10 dB or below a uniform pattern can be optimal. In turn, for high level of noise attenuation a uniform distribution is far from optimal. With a fine grid, the distribution based on the Gauss-Legendre quadrature significantly improves the noise reduction with the increase of the number of controls, surpassing the shifted uniform distribution. It turns out that for NASC the optimal distribution patterns for controls and sensors can be different. As a result, a combined distribution pattern can highly reduce the number of sensors in contrast to the plane shifted uniform distribution. It has been also shown that two controls or sensors per wavelength is sufficient for essential noise attenuation. In addition, it has been obtained that the optimized nonlocal control can reach the level of local control with respect to the minimal number of controls required.

In the future work, the algorithms considered above will be extended to bro-

adband noise attenuation.

7 Acknowledgement

The authors are grateful to the unknown referees for useful remarks which improved the quality of the paper.

References

[1] B. B. Baker and E. T. Copson. *The mathematical theory of Huygens' principle*. Oxford: Clarendon Press, 1939.

[2] G. Canevet. Active sound absorption in an air conditioning duct. *J Sound Vib*, 58(3):333–345, 1978.

[3] L. Ding and X. Cheng. *Method of numerical calculation*. 2nd ed. Beijing Institute of Technology Press, 2011.

[4] N. Epain and E. Friot. Active control of sound inside a sphere via control of the acoustic pressure at the boundary surface. *J Sound Vib*, 299(3):587–604, 2007.

[5] M. V. Fedoryuk. An unsteady problem of active noise suppression. *Acoust J*, 22:439–443, 1976.

[6] C. Hansen, S. Snyder, X. Qiu, L. Brooks, and D. Moreau. *Active control of noise and vibration*. 2nd ed. CRC press, 2012.

[7] X. Huang, H.and Qiu and J. Kang. Active noise attenuation in ventilation windows. *J Acoust Soc Am*, 130(1):176–188, 2011.

[8] A. Jakob and M. Möser. Active control of double-glazed windowspart I: Feedforward control. *Applied Acoustics*, 64(2):163–182, 2003.

[9] Jakob, A. and Möser, M. Active control of double-glazed windows. part II: Feedback control. *Appl Acoust*, 64(2):183–196, 2003.

[10] T. Kletschkowski. *Adaptive feed-forward control of low frequency interior noise*. Springer Netherlands, 2012.

[11] S. I. Konyaev, V. I. Lebedev, and M. V. Fedoryuk. Discrete approximation of a spherical Huygens surface. *Soviet Physics Acoustics*, 23:373–374, 1977.

[12] S. I. Konyaev, V. I. Lebedev, and M. V. Fedoryuk. Discrete approximation of spherical and ellipsoidal Huygens surfaces. *Soviet Physics Acoustics*, 25:887–892, 1979.

[13] B. Kwon and Y. Park. Active window based on the prediction of interior sound field: experiment for a band-limited white noise. In *INTER-NOISE and NOISE-CON Congress and Conference Proceedings*, volume 2011, pages 443–446. Institute of Noise Control Engineering, 2011.

[14] J. Landaluze, I. Portilla, J. M. Pagalday, A. Martinez, and R. Reyero. Application of active noise control to an elevator cabin. *Control Eng Pract*, 11(12):1423–1431, 2003.

[15] H. Lim, S. V. Utyuzhnikov, Y. W. Lam, and L. Kelly. Potential-based methodology for active sound control in three dimensional settings. *J Acoust Soc Am*, 136(3):1101–1111, 2014.

[16] H. Lim, S. V. Utyuzhnikov, Y. W. Lam, and A. Turan. Multi-domain active sound control and noise shielding. *J Acoust Soc Am*, 129(2):717–725, 2011.

[17] H. Lim, S. V. Utyuzhnikov, Y. W. Lam, A. Turan, M. R. Avis, V. S. Ryaben'kii, and S. V. Tsynkov. Experimental validation of the active noise control methodology based on difference potentials. *AIAA J*, 47(4):874–884, 2009.

[18] J. Loncarič, V. S. Ryaben'kii, and S. V. Tsynkov. Active shielding and control of noise. *SIAM J Appl Math*, 62(2):563596, 2001.

[19] J. Loncarič and S. V. Tsynkov. Optimization of acoustic source strength in the problems of active noise control. *SIAM J Appl Math*, 63:1141–1183, 2003.

[20] J. Loncarič and S. V. Tsynkov. Optimization of power in the problem of active control of sound. *Math Comput Simul*, 65:323–335, 2004.

[21] P. Lueg. Process of silencing sound oscillations, 1936.

[22] G. D. Malyuzhinets. An unsteady diffraction problem for the wave equation with compactly supported right-hand side. *Proc USSR Acad Sci*, pages 124–139, 1971.

[23] M. Muhammad and M. Mori. Double exponential formulas for numerical indefinite integration. *J Comput Appl Math*, 161(2):431–448, 2003.

[24] P. A. Nelson and J. Elliott, S. *Active control of sound*. Academic Press, 1992.

[25] E. A. Ntumy and S. V. Utyuzhnikov. Active sound control in 3D bounded regions. *Wave Motion*, 51(2):284–295, 2014.

[26] E. A. Ntumy and S. V. Utyuzhnikov. Active sound control in composite regions. *Appl Numer Math*, 93:242–253, 2015.

[27] C. D. Petersen, R. Fraanje, B. S. Cazzolato, A. C. Zander, and C. H. Hansen. A Kalman filter approach to virtual sensing for active noise control. *Mech Syst Signal Process*, 22(2):490–508, 2008.

[28] V. S. Ryaben'kii. *Method of difference potentials and its applications*. Berlin: Springer-Verlag, 2002.

[29] V. S. Ryaben'kii. Model of real-time active noise shielding of a given subdomain subject to external noise sources. *Comput Math Math Phys*, 51(3):444–454, 2011.

[30] V. S. Ryaben'kii, S. V. Tsynkov, and S. V. Utyuzhnikov. Inverse source problem and active shielding for composite domains. *Appl Math Lett*, 20(5):511–515, 2007.

[31] V. S. Ryaben'kii, S. V. Tsynkov, and S. V. Utyuzhnikov. Active control of sound with variable degree of cancellation. *Appl Math Lett*, 22(12):1846–1851, 2009.

[32] V. S. Ryaben'kii and S. V. Utyuzhnikov. Active shielding model for hyperbolic equations. *IMA J Appl Math*, 71(6):924–939, 2006.

[33] V. S. Ryaben'kii and S. V. Utyuzhnikov. Differential and finite-difference problems of active shielding. *Appl Numer Math*, 57(4):374–382, 2007.

[34] V. S. Ryaben'kii, S. V. Utyuzhnikov, and A. Turan. On the application of difference potential theory to active noise control. *Adv Appl Math*, 40(2):194–211, 2008.

[35] H. Takahasi and M. Mori. Double exponential formulas for numerical integration. *Publ Res Inst Math Sci*, 9(3):721–741, 1973.

[36] S. V. Tsynkov. On the definition of surface potentials for finite-difference operators. *J Sci Comput*, 18:155–189, 2003.

[37] S. V. Utyuzhnikov. Generalized Calderon-Ryaben'kii's potentials. *IMA J Appl Math*, 74(1):128–148, 2008.

[38] S. V. Utyuzhnikov. Active wave control and generalized surface potentials. *Adv Appl Math*, 43(2):101–112, 2009.

[39] S. V. Utyuzhnikov. Non-stationary problem of active sound control in bounded domains. *J Comput Appl Math*, 234(6):1725–1731, 2010.

[40] S. V. Utyuzhnikov. Nonlinear problem of active sound control. *J Comput Appl Math*, 234(1):215–223, 2010.

[41] S. V. Utyuzhnikov. Real-time active wave control with preservation of wanted field. *IMA J Appl Math*, 79(6):1126–1138, 2013.

[42] S. V. Utyuzhnikov. A practical algorithm for real-time active sound control with preservation of interior sound. *Comput Fluids*, 157:175–181, 2017.

[43] J. E. Williams. Review lecture-anti-sound. *Proc R Soc Lond A*, 395(1808):6388, 1984.

[44] C. Zhou and S. V. Utyuzhnikov. Real-time active noise control with preservation of desired sound. *Appl Acoust*, 157:106971, 2020.

[45] C. Zhou and S. V. Utyuzhnikov. Study of the nonlocal active sound control with preservation of desired field in time domain. *J Acoust Soc Am*, 148(6):3886, 2020.

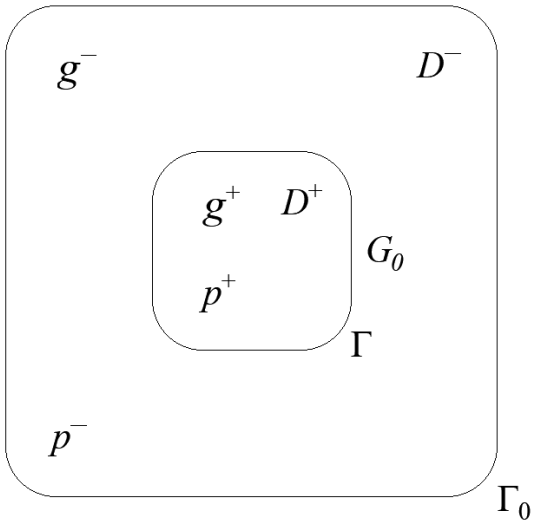

Fig. 1. Sketch of region for local control

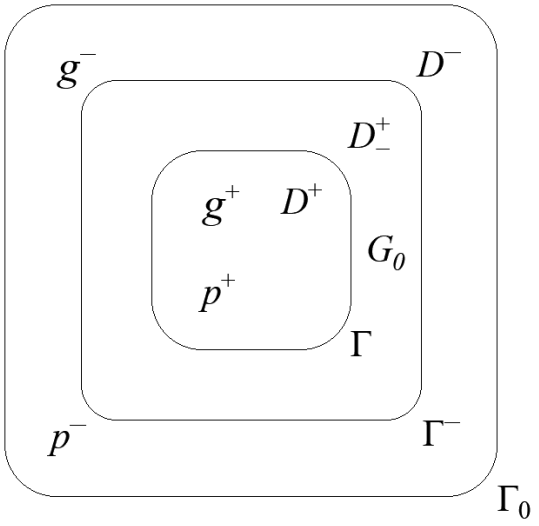

Fig. 2. Sketch of region for nonlocal control

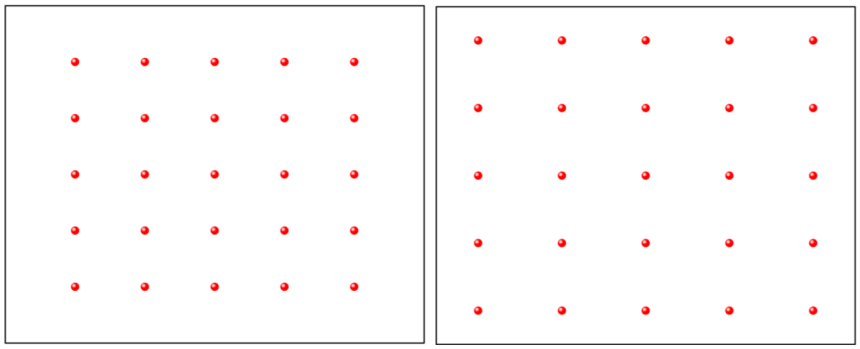

(a) OU distribution (b) SU distribution

Fig. 3. Uniform 5×5 grid on cube side

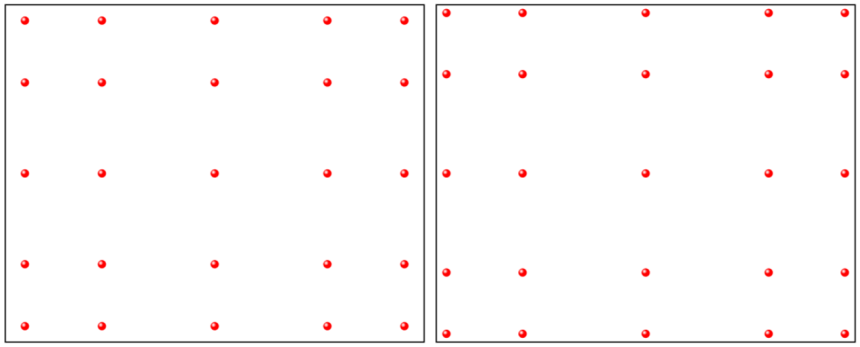

(a) GL distribution (b) CG1 distribution

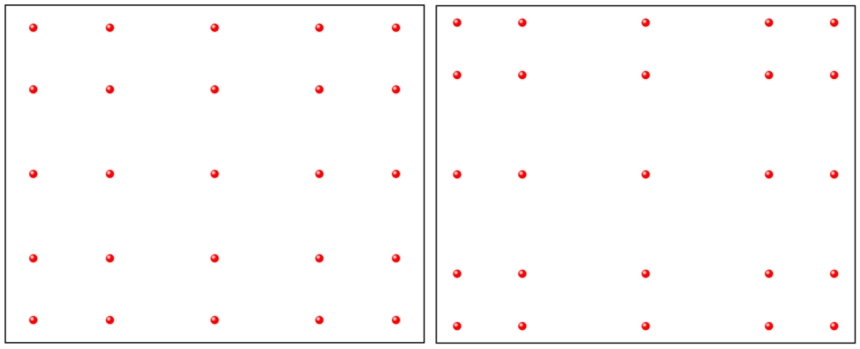

(c) CG2 distribution (d) TS distribution

Fig. 4. Nonuiform 5×5 grid

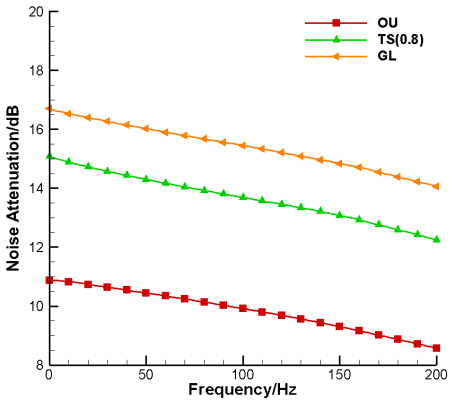

(a) GL, TS and OU distributions

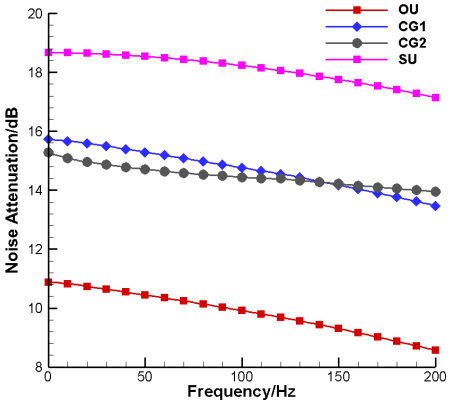

(b) CG, SU and OU distributions

Fig. 5. Noise attenuation by local control without desired sound ($n_c = 3$)

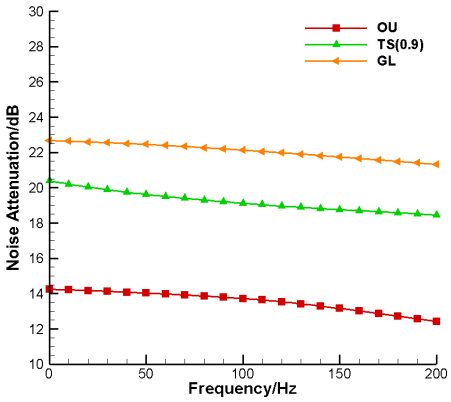

(a) GL, TS and OU distributions

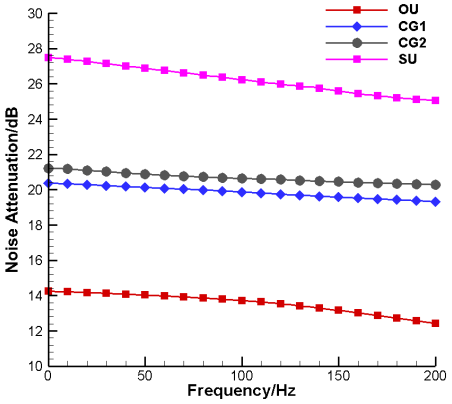

(b) CG, SU and OU distributions

Fig. 6. Noise attenuation by local control without desired sound ($n_c = 5$)

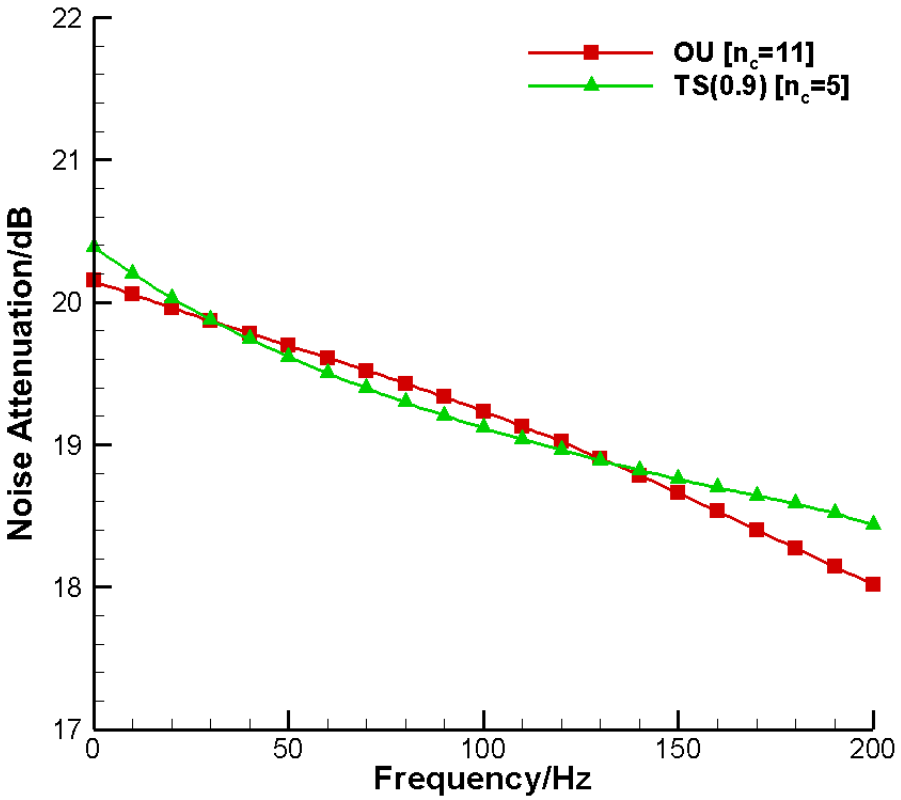

Fig. 7. Different distributions with the same level of attenuation by local control

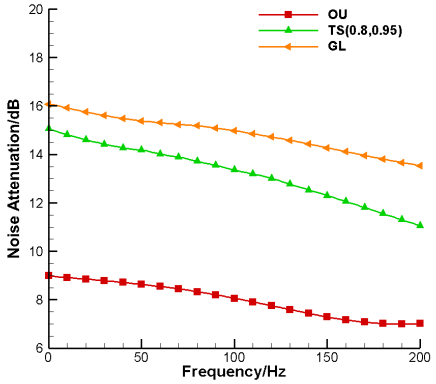

(a) GL, TS and OU distributions with desired sound

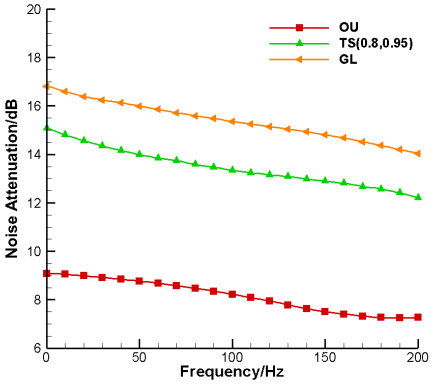

(b) GL, TS and OU distributions without desired sound

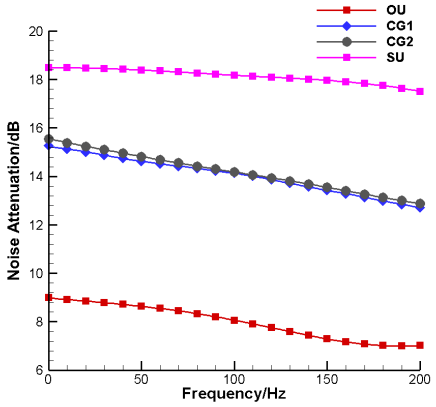

(c) CG, SU and OU distributions with desired sound

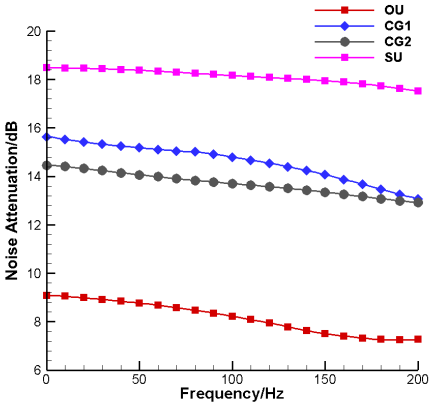

(d) CG, SU and OU distributions without desired sound

Fig. 8. Noise attenuation by nonlocal control ($n_c = 3$)

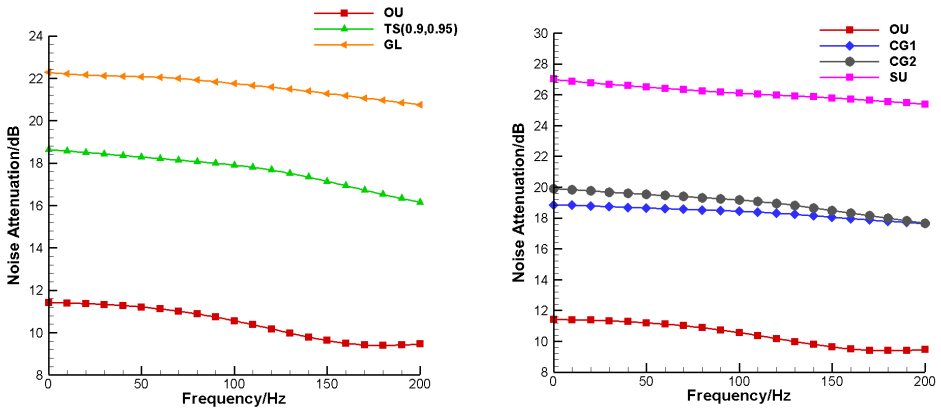

(a) GL, TS and OU distributions with desired sound

(b) CG, SU and OU distributions with desired sound

Fig. 9. Noise attenuation by nonlocal control ($n_c = 5$)

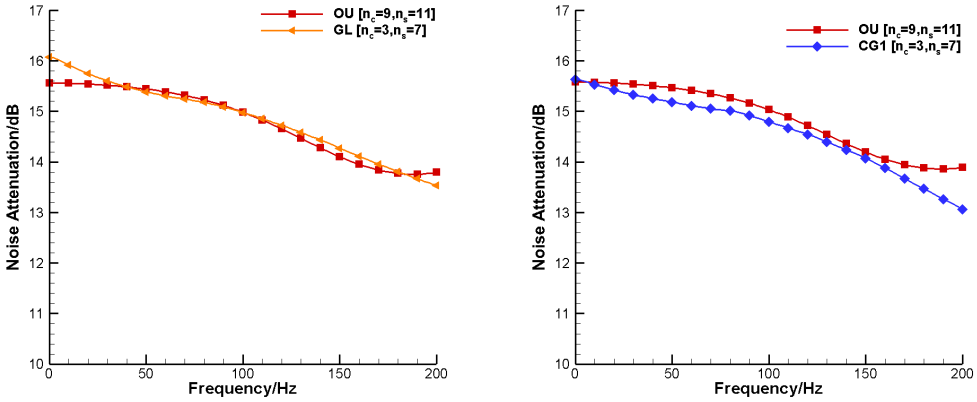

(a) GL and OU distributions with desired sound

(b) CG1 and OU distributions without desired sound

Fig. 10. Different distributions with the same level of noise attenuation by nonlocal control

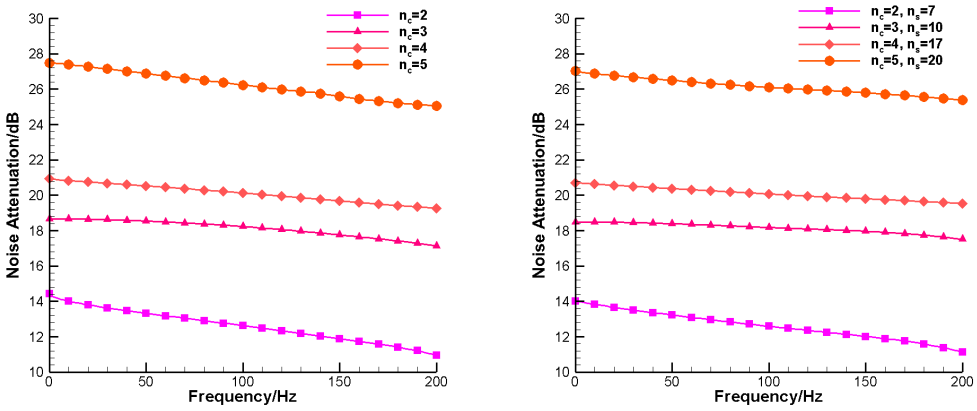

(a) SU distributions by local control without desired sound

(b) SU distributions by nonlocal control with desired sound

Fig. 11. Noise attenuation with SU for $n_c = 2, 3, 4, 5$

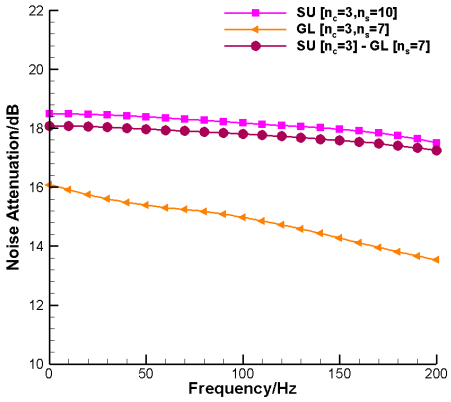

(a) $n_c = 3$ with desired sound

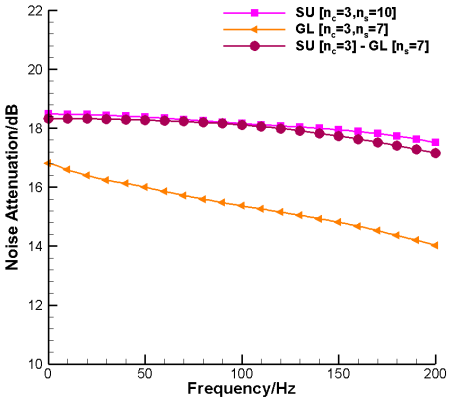

(b) $n_c = 3$ without desired sound

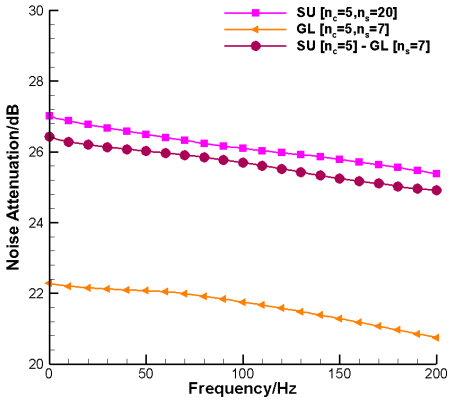

(c) $n_c = 5$ with desired sound

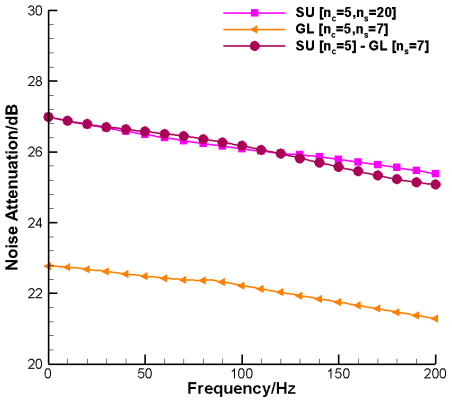

(d) $n_c = 5$ without desired sound

Fig. 12. Noise attenuation by nonlocal control with different distributions

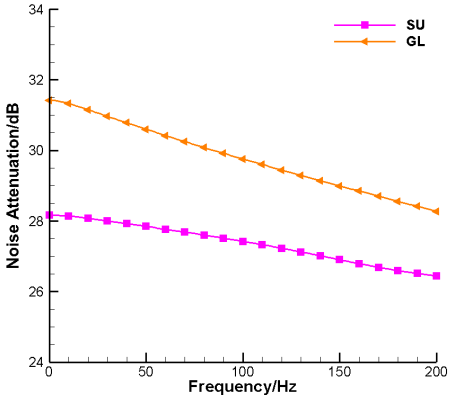

(a) Local control ($n_c = 6$)

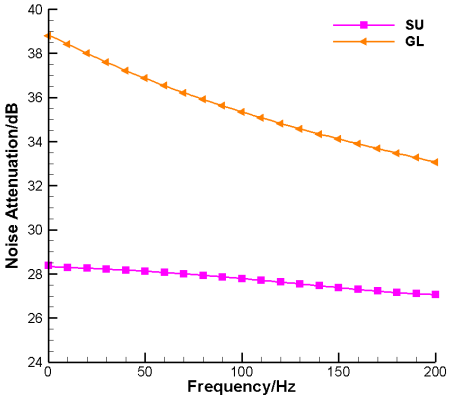

(b) Local control ($n_c = 7$)

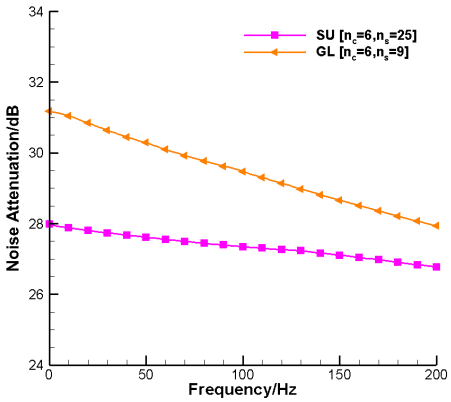

(c) Nonlocal control with desired sound ($n_c = 6$)

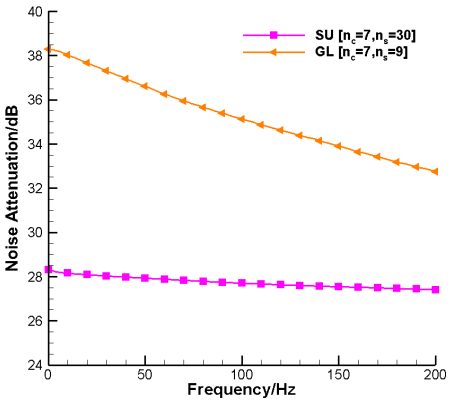

(d) Nonlocal control with desired sound ($n_c = 7$)

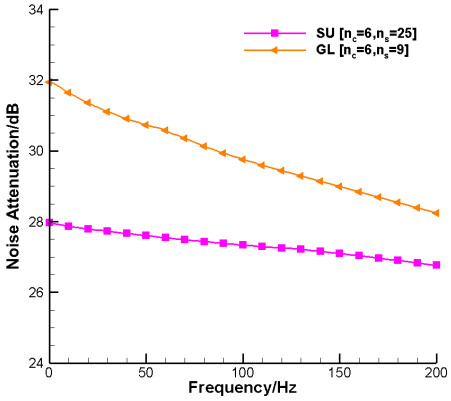

(e) Nonlocal control without desired sound ($n_c = 6$)

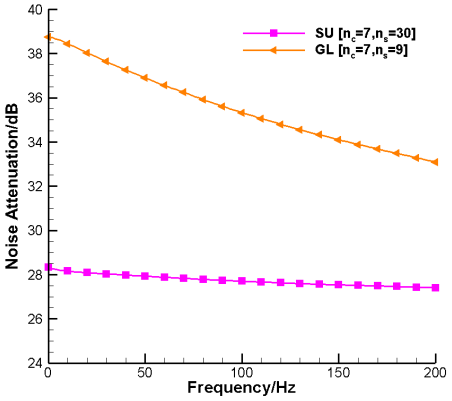

(f) Nonlocal control without desired sound ($n_c = 7$)

Fig. 13. Noise attenuation by GL and SU distributions with fine grid

Table 1

Local control without desired sound

Number of controls per direction per wavelength	Frequency /Hz	Wavelength /m	Noise Attenuation/dB					
			OU	GL	CG1	CG2	TS(0.9)	SU
4	245.00	1.40	10.19	16.25	14.22	17.25	13.80	21.23
3	326.67	1.05	8.32	12.30	10.80	14.58	10.92	19.05
2	490.00	0.70	6.82	6.62	6.29	8.43	7.09	10.91

Table 2

Nonocal control with desired sound

Number of controls or sensors per direction per wavelength	Frequency /Hz	Wavelength /m	Noise Attenuation/dB					
			OU	GL	CG1	CG2	TS(0.9,0.95)	SU
4	245.00	1.40	8.64	16.25	14.17	17.05	12.88	20.21
3	326.67	1.05	4.77	12.36	10.82	14.46	10.37	17.70
2	490.00	0.70	5.97	4.41	2.89	6.66	2.25	11.84

Table 3

Nonocal control without desired sound

Number of controls or sensors per direction per wavelength	Frequency /Hz	Wavelength /m	Noise Attenuation/dB					
			OU	GL	CG1	CG2	TS(0.9,0.95)	SU
4	245.00	1.40	8.57	16.25	14.18	17.05	12.86	20.30
3	326.67	1.05	4.71	12.36	10.83	14.45	10.36	17.65
2	490.00	0.70	5.85	4.32	3.01	6.70	2.21	11.50

Appendix

A Gauss-Legendre quadrature

In 1D case, the Gauss quadrature reads:

$$\int_{a'}^{b'} \rho(x) f(x) dx \approx \sum_{k=1}^{n} A_k f(x_k).$$

Here, $[a', b']$ is an arbitrary integration interval; the weight function $\rho(x)$ in the integrand $\rho(x)f(x)$ varies for different quadratures; x_k represents a k-th Gauss point, where k=1, ..., n; A_k is the weight corresponding to Gauss points x_k.

On the definition this quadrature is exact for polynomials with degree up to $2n - 1$.

Thus, the quadrature condition is the following:

$$\int_{a'}^{b'} \rho(x) q(x) p_n(x) dx = 0,$$

where $p_n(x) = \prod_{k=1}^{n} (x - x_k)$ is a polynomial with degree n and the degree of arbitrary polynomials $q(x)$ is no more than $n - 1$. Then, x_k and A_k can be found.

For the Gauss-Legendre quadrature, the weight function $\rho(x) \equiv 1$ and the integration interval is $[-1, 1]$, the Gauss points x_k are zeros of the Legendre polynomials:

$$\begin{aligned} &L_0(x) = 1, \\ &L_n(x) = \frac{1}{2^n n!} \frac{d^n}{dx^n} [(x^2 - 1)^n], \quad (n = 1, 2, ...). \end{aligned}$$

The corresponding weights A_k which comprise the derivation of Legendre polynomials ${L_n}'(x_k)$ at the Gauss points are given by

$$A_k = \frac{2}{(1-x_k^2)[{L_n}'(x_k)]^2}, \quad (k = 1, 2, ..., n).$$

To extend the Gauss-Legendre quadrature to arbitrary finite integration interval $[a, b]$, the modifications toward x_k and A_k should be made. Then, we obtain new Gauss points x_{ak} and weights A_{ak}:

$$x_{ak} = \frac{b-a}{2}x_k + \frac{a+b}{2},$$
$$A_{ak} = \frac{b-a}{2}A_k.$$

Here, $(b-a)/2$ is the scale factor between intervals, and $(a+b)/2$ is the translation distance between the middle points of two intervals.

The extension of 1D integration to a 2D case for a rectangular domain is straightforward. If we select the Cartesian coordinate system with the axes parallel to the adjacent sides of the domain, then the coordinates of Gauss points can be immediately found according to the length of sides. It is worth mentioning that the weight of Gauss points in 2D is the product of 1D weights.

B Chebyshev-Gauss quadrature

The Chebyshev-Gauss quadrature [3] is another type of quadrature within interval $[-1, 1]$. It is worth noting that there are Chebyshev-Gauss quadratures of the first and second forms.

In the first form of Chebyshev-Gauss (CG1) quadrature, the weight function

$\rho(x) = 1/\sqrt{1-x^2}$. The Gauss point x_k coincide with the zeros of Chebyshev polynomials $T_n(x)$ of the first kind:

$$T_n(x) = \cos(n \arccos x), \quad (n = 0, 1, 2, ...).$$

Then, we have

$$x_k = \cos(\frac{2k-1}{2n}\pi),$$
$$A_k = \frac{\pi}{n}, \quad (k = 1, 2, ..., n).$$

In the second Chebyshev-Gauss (CG2) quadrature, the weight function $\rho(x) = \sqrt{1-x^2}$. The Gauss points x_k are given by the zeros of Chebyshev polynomials $U_n(x)$ of the second kind:

$$U_n(\cos x) \sin x = \sin((n+1)x), \quad (n = 0, 1, 2, ...).$$

Thus,

$$x_k = \cos(\frac{k}{n+1}\pi),$$
$$A_k = \frac{\pi}{n+1}\sin^2(\frac{k}{n+1}\pi), \quad (k = 1, 2, ..., n).$$

The approach to extend to arbitrary finite integration interval $[a, b]$ and 2D case is the same as described above.

C Tanh-Sinh quadrature

The Tanh-Sinh quadrature [23, 35] is also known as the Double Exponential (DE) formula. Initially, it was utilized to transform an original integration in

infinite interval $(-\infty, +\infty)$ to finite interval $[-1, 1]$. Then, the integration in finite interval $[-1, 1]$ can be approximated by infinite summation:

$$\int_{-1}^{1} f(x)dx = \sum_{k=-\infty}^{\infty} A_k f(x_k).$$

In this case, we have

$$\begin{aligned} x_k &= \tanh(\frac{1}{2}\pi \sinh kh), \\ A_k &= \frac{\frac{1}{2}h\pi \cosh kh}{\cosh^2(\frac{1}{2}\pi \sinh kh)}, \quad (k = -n, ..., -1, 0, 1, ..., n), \end{aligned}$$

where parameter h represents a uniform step size in the original integration, which corresponds to a nonuniform step size in the integration transformed. After transformation, the step size in the new integration rapidly decreases and converges to zero with the increase value of $|x_k|$.

It is worth mentioning some important properties of the Tanh-Sinh quadrature. The original integration rapidly converges in an interval around the origin point. As can be seen, the x_k and A_k are symmetrical with respect to the origin. In addition, if point x_k is fixed, the increase of the step size h must lead to decrease of k. Moreover, x_k converges to 1 or -1 and A_k converges to zero with the increase of $|k|$. In other words, the Tanh-Sinh quadrature is quite insensitive to the behavior of the endpoints.

In this problem, the number of points is small and the suitable step size h, which affects the final result, is unknown at first. Since we know that the endpoints should be near to 1 or -1, we introduce coefficient α near to 1. Then, the following formula is reversely used to calculate h with given α:

$$\tanh(\frac{1}{2}\pi \sinh nh) = \alpha$$

Modifying α, we can obtain suitable h for best final results.